Cavitation clouds created by shock scattering from bubbles during histotripsy

Adam D. Maxwell,[a] Tzu-Yin Wang, Charles A. Cain, and J. Brian Fowlkes
Department of Biomedical Engineering, University of Michigan, 1107 Gerstacker Building,
2200 Bonisteel Boulevard, Ann Arbor, Michigan 48109

Oleg A. Sapozhnikov and Michael R. Bailey
Center for Industrial and Medical Ultrasound, Applied Physics Laboratory, 1013 NE 40th Street,
University of Washington, Seattle, Washington 98105

Zhen Xu
Department of Biomedical Engineering, University of Michigan, 1107 Gerstacker Building,
2200 Bonisteel Boulevard, Ann Arbor, Michigan 48109

Histotripsy is a therapy that focuses short-duration, high-amplitude pulses of ultrasound to incite a localized cavitation cloud that mechanically breaks down tissue. To investigate the mechanism of cloud formation, high-speed photography was used to observe clouds generated during single histotripsy pulses. Pulses of $5-20$ cycles duration were applied to a transparent tissue phantom by a 1-MHz spherically focused transducer. Clouds initiated from single cavitation bubbles that formed during the initial cycles of the pulse, and grew along the acoustic axis opposite the propagation direction. Based on these observations, we hypothesized that clouds form as a result of large negative pressure generated by the backscattering of shockwaves from a single bubble. The positive-pressure phase of the wave inverts upon scattering and superimposes on the incident negative-pressure phase to create this negative pressure and cavitation. The process repeats with each cycle of the incident wave, and the bubble cloud elongates toward the transducer. Finite-amplitude propagation distorts the incident wave such that the peak-positive pressure is much greater than the peak-negative pressure, which exaggerates the effect. The hypothesis was tested with two modified incident waves that maintained negative pressure but reduced the positive pressure amplitude. These waves suppressed cloud formation which supported the hypothesis. © 2011 Acoustical Society of America. [DOI: 10.1121/1.3625239]

I. INTRODUCTION

Cavitation plays an important role in the development of focused ultrasound therapies. Inertial cavitation can manifest as either an undesirable side effect of treatment or a therapeutic mechanism of its own. For instance, cavitation during lithotripsy facilitates stone fracture,[1,2] but is also associated with concomitant mechanical damage and hemorrhage in the surrounding kidney tissue.[3,4] Methods to control cavitation during lithotripsy have been employed, including waveform modification to suppress cavitation[3,5] and dual-head devices which use spatially dependent timing between pulses to either enhance and mitigate cavitation.[6] Control of cavitation is also desirable in high-intensity focused ultrasound (HIFU) thermal therapy, where cavitation can promote heating to shorten treatment time,[7] but the random position of individual nuclei can also confound expected focal heating patterns.[8]

Cavitation is a primary mechanism of histotripsy, a form of mechanical ultrasound ablation therapy that applies short-duration, highly nonlinear, focused pulses to perform targeted breakdown of unwanted tissue.[9,10] Under this modality, a cavitation cloud is generated within the focal zone of the transducer.[11] The cavitation associated with histotripsy effects is described as a "bubble cloud," which has only been observed at pressure excursions much greater than inertial cavitation thresholds determined for similar frequency and pulse lengths in water.[12,13] A bubble cloud may be initiated during any pulse in a sequence of thousands of pulses,[12] although all incident pulses are essentially identical. This observation is evidence that bubble cloud initiation is a probabilistic phenomenon. However, once a cloud is generated, it is maintained by each pulse if the pulse repetition period is shorter than the time for the bubbles that make up the cloud to dissolve.[14,15] Since tissue disruption in histotripsy is not observed without first initiating a bubble cloud in the tissue, an understanding of how cavitation clouds form is of fundamental importance to designing effective transducers and strategies for histotripsy therapy.

Cloud cavitation at therapeutic ultrasound intensities has been observed in several forms in water, under conditions of both CW excitation[16–18] and lithotripsy shockwaves.[2,19–21] Cavitation clouds generated using focused ultrasound have been observed to form transiently in water with CW sonication at 2.5 MHz by Willard[17] and at 1 MHz by Neppiras and Coakley.[18] More recently, Sankin and Teslenko[20] have generated cavitation clouds in distilled water using a strong lithotripter

[a] Author to whom correspondence should be addressed. Electronic mail: adamdm@umich.edu

shockwave. In their study, individual cavitation bubbles were apparent at low pressures, but cavitation clouds appeared consistently when a threshold of approximately 33 MPa peak negative pressure was exceeded.[20,22] While it was found that cavitation clouds could be excited by direct action of the tensile tail of a shockwave, clouds were also observed to form by the reflection and inversion of the compressive shock from the water–air interface at the top of the tank. In an *in vivo* scenario, such cavitation may occur as a result of the reflection of strongly nonlinear waves from pre-existing gas bodies in tissues such as lung or intestine. Experimentally, Bailey *et al.*[23] found that isolated 1-MPa positive-pressure pulses caused equivalent hemorrhage as 1-MPa negative pressure pulses in tissue structures containing gas bodies. Church[24] proposed this could be due to cavitation activity related to the reflection and inversion of the pulse from the gas body and that the true achievable negative pressure would be the peak-to-peak incident pressure.

Based on observations and experiments reported herein using high-speed photography, we hypothesize that cavitation clouds in histotripsy evolve by reflection of a positive wave from single cavitation bubbles. Incidence of a shock front on a bubble within the central portion of the focus backscatters a negative-pressure pulse. This reflection incites cavitation proximal to the initial bubble, which produces a larger effective scattering surface for the next shock in the incident pulse. Thus, the process is self-reinforcing, being terminated only at the end of the pulse or when the cloud extends outside of the focus, where the pressure is too low to create sufficient scattering. Both the compressive and rarefaction phases of the wave, as well as the degree of nonlinear distortion, play a role in generating cavitation clouds under this mechanism. In this article, we describe the formation of bubble clouds observed during single pulses at the focus of a 1-MHz ultrasound transducer in a gelatin tissue-mimicking phantom using high-speed photography. We then evaluate the hypothesized mechanism of shock scattering by three experiments. In the first experiment, we compare the region where bubble clouds form with the dimensions of the positive and negative pressure zones of the focus. In the second experiment, two transducers which produce the same peak negative focal pressure and frequency but different nonlinear waveform distortion are compared to evaluate their effect on producing clouds. In the third experiment, the shocks are acoustically filtered from the waveform while maintaining the same peak negative pressure to evaluate the importance of shock amplitude in generating clouds.

II. METHODS

A. Experimental apparatus

Bubble clouds were generated in tissue mimicking phantoms composed of gelatin, which was chosen because of its high optical clarity for photography and similarity of its properties to those of soft tissue.[25] Type-A gelatin from porcine skin (G2500, Sigma-Aldrich, St. Louis, MO) and deionized water were combined at a ratio of 7 g gelatin per 100 mL water and then heated on a hot plate to melt the gelatin completely into solution. The mixture was placed in a degassing chamber at a vacuum of 74 kPa for 30 min. Next, the solution was carefully poured into a polycarbonate housing. The housing had one side open for ultrasound exposure and the opposite side had an acoustic window of 25-μm thickness polycarbonate. After all bubbles were skimmed from the surface of the molten gelatin, the phantom placed in refrigeration at 4 °C until solidified. Two hours prior to use, phantoms were submerged in degassed water at room temperature.

A high-speed framing camera (SIM 02, Specialized Imaging, Hertfordshire, UK) was used to observe bubble cloud formation at the focus of a histotripsy transducer during sonication. The camera is capable of capturing 16 frames at rates up to 2×10^8 frames per second (fps). Frame rates used in this study were between $5 \times 10^4 - 10^7$ fps. The transducer was a piezocomposite bowl of 10 cm aperture and 9 cm focal length (radius of curvature), with a 5 cm diameter concentric hole in the center (Imasonic, Voray sur l'Ognon, France). The working frequency was 1 MHz. The transducer was placed in a tank of filtered, degassed water at room temperature, attached to a three-axis motorized positioning system. The transducer was driven by a class D amplifier with matching network constructed in-house.[26] The tissue phantom was positioned such that the entire focus of the transducer was within the phantom. The camera was positioned to acquire axial-lateral images of the focal region of the transducer (Fig. 1). Tominon macro-bellows lenses (Kyocera Optics, Nagano, Japan) were used to control magnification, focusing, and camera aperture. Images were backlit using one of two xenon flashlamps for either short-term or long-term exposure (IS 300 and ADA 500, Adapt Electronics, Hertsfordshire, UK). The flash lamp was coupled into a fiber optic bundle, whose output was passed through a convex lens to control the light beam diameter. This backlit shadowgraph method was used instead of front- or side-lighting in order to view ultrasound propagation and interaction with the cavitation, and to minimize the exposure time of the camera. The transducer was driven with a single pulse of 5 to 20 cycles
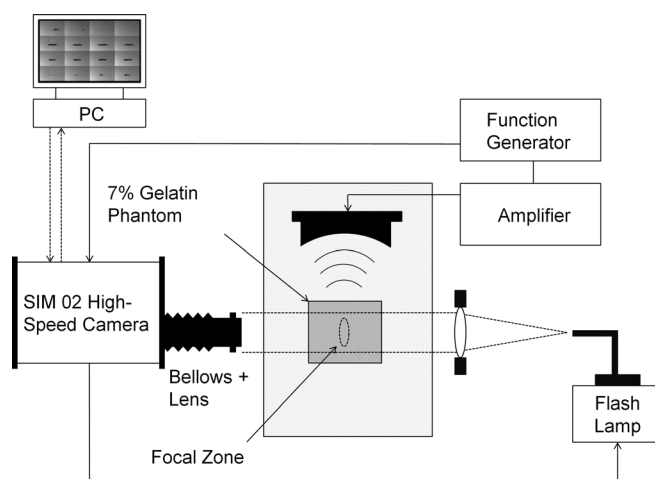

FIG. 1. Apparatus for high-speed imaging of histotripsy bubble clouds. A fiber-coupled flash lamp was used to back-illuminate images captured by the camera. An ultrasound transducer placed in the water tank was focused into a gelatin-based tissue-mimicking phantom. The transducer was driven by a class D amplifier with matching circuit. A function generator was used to control the amplifier output and trigger the camera, which in turn triggered the flash lamp.

duration and the camera recorded images as the pulse passed through the focal zone. For all experiments where the pressure levels are not explicitly specified in the results, each pulse had a peak positive/negative pressure of 85/19 MPa. Because cavitation damage changes the mechanical properties of the tissue phantom, the focus of the transducer was moved to a new location in the phantom for each pulse applied.

Ultrasound pressure waveforms were measured in degassed water using a fiber-optic hydrophone constructed in house.[27] The hydrophone's frequency response was calibrated by substitution comparison with a reference piezoelectric hydrophone (HGL-0085, Onda Corporation, Sunnyvale, CA). The measured waveforms were corrected using a deconvolution procedure to account for the frequency response of the hydrophone. While the measurements were not recorded in the tissue phantom, they provide a good estimate of the focal pressure in the phantom, since the attenuation of the gelatin is low. Measurements were recorded with short pulses (three cycles) to limit the potential for cavitation on the hydrophone and its confounding of the signal. It was found that the transducer output reached full amplitude by the third cycle, thus the peak pressure values recorded are the same for the longer pulses used in this study.

B. Evaluation of cloud formation mechanism

Three experiments were performed to evaluate the mechanism for bubble cloud initiation: The hypothesis is that bubble clouds are created when the incident positive pressure phase of the shocked pulse reflects and inverts from a single cavitation bubble. This negative transient backscattered wave incites a cloud of cavitation bubbles proximal to the scatterer.

1. Cloud formation position

If cloud formation is dependent on the positive pressure, the initial position of cloud formation will be limited to the positive-pressure focal region instead of the negative-pressure focal region. Histotripsy pulses are distorted from a sinusoidal shape because of nonlinear propagation. A typical pulse contains multiple cycles, each cycle consisting of a steep shock front with a high-amplitude, positive-pressure phase followed by a lower-amplitude, negative-pressure phase (Fig. 2). The waveform displays strong asymmetry, in that the peak positive pressure of the pulses is several times greater than the peak negative pressure because of the combined effects of nonlinear propagation and diffraction. The higher harmonics of the wave focus within a smaller zone and thus the volume over which the pulse has a high positive pressure is limited to a small region in the center of the focus.[28,29] The peak negative pressure is distributed over a significantly larger region, similar to that defined by linear propagation when the waveform is sinusoidal. If scattering of the positive phase of the wave is the mechanism of cloud initiation, then it is expected that cloud initiation will occur only within the narrow central region of the focus where the positive pressure is high. To test this, we recorded the lateral and axial locations of the single bubbles from which clouds began to form.
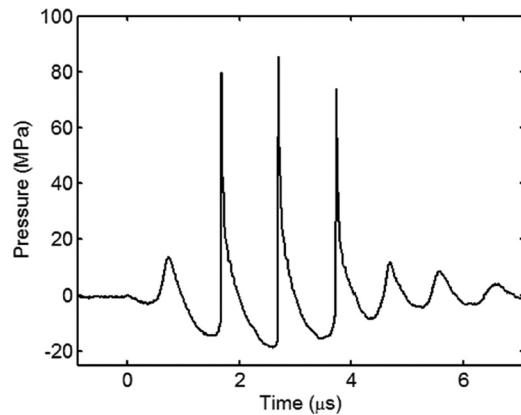

FIG. 2. A 3-cycle focal pressure waveform of the histotripsy transducer used to generate bubble clouds. The waveforms are asymmetric with a larger positive-pressure excursion than negative-pressure excursion as a result of nonlinear acoustic propagation and diffraction. Pulse lengths of 5–20 cycles were used in this study for generating clouds.

2. Cloud formation with different waveform asymmetry

If bubble cloud formation is dependent on scattering of the positive pressure phase, then a transducer outputting a lower positive pressure level for a given negative pressure level, i.e., a lower ratio $p_+/|p_-|$, will have a higher threshold of negative pressure for bubble cloud formation. The waveform asymmetry can be characterized by the ratio between peak positive and peak negative pressures $p_+/|p_-|$. The waveform asymmetric distortion is always pronounced in nonlinear acoustic beams because of the combined action of acoustic nonlinearity and diffraction, which results in $p_+ > |p_-|$.[29] In the case of focused beams, the asymmetry is usually strongest at the focus and depends on the transducer F number (ratio of the transducer focal length to diameter). In this study, a 1-MHz, F number 0.9 transducer (diameter $= 10$ cm, focal length $= 9$ cm) and another 1-MHz, F number 0.6 transducer (diameter $= 17$ cm, focal length $= 10$ cm) were used to generate different levels of waveform asymmetry for a given peak negative pressure value. For the pressure range applied in this study, the transducer with a lower F number produced a waveform with a lower $p_+/|p_-|$ ratio. The -6 dB negative pressure lateral beamwidth is 2.2 mm and the axial beamwidth is 15 mm for the F number $= 0.9$ transducer. The lateral beamwidth is 1.2 mm and the axial beamdwidth is 7 mm for the F number $= 0.6$ transducer. For linear propagation, the peak positive beamwidth is the same as that for peak negative pressure. However, at higher amplitude, the positive pressure beamwidth is reduced because of stronger focusing of harmonics.

The negative pressure threshold at which bubble clouds were first observed to form was recorded with both transducers. Additionally, the probability of bubble cloud formation was recorded over a range of pressure levels using 15-cycle pulses for each transducer. Individual pulses were applied to the tissue phantom, and the presence or absence of a cloud on the high-speed camera image was noted in each case. The probability was defined as the fraction of pulses that generated a cavitation cloud visible on the high-speed camera images.

3. Cloud formation with reduced shock amplitude

If shockwave scattering is the mechanism of cloud formation, then reduction of only the peak positive pressure of the incident wave will suppress cloud formation. In order to accomplish this effect, thin brass sheets were placed between the transducer and focus aligned perpendicular to the propagation axis. The sheets act as a low-pass filter, primarily reducing the harmonics of the nonlinear wave. The outcome is that the positive peak focal pressure is more greatly reduced than the negative peak focal pressure when the sheets' thickness and material are chosen appropriately. The sheets must be placed near the focus to allow nonlinear distortion to develop before impinging on the filter. Once the filter was in place, the driving voltage on the transducer was increased to reach the same peak negative focal pressure as the original incident wave without the filter. If shock scattering is the mechanism of bubble cloud formation, it is expected that bubble clouds will be suppressed under the modified waveform with reduced levels of harmonics, while single bubbles should still appear within the focal region. The appropriate thickness and material were determined by testing different sheets with the hydrophone at the focus and recording the waveforms with each in position. For this experiment, the filter consisted of three brass sheets each 0.075 mm thickness spaced 0.5 mm apart, placed about 1 cm proximal of the focus center. The filter was assembled under water to ensure no air was trapped between the sheets. The pressure distribution in the plane normal to the acoustic axis was recorded with and without the sheets in place to ensure the peak pressure levels were measured at the true maximum. After recording pressure levels, the sheets were attached to the front of the tissue phantom holder, and the focus was positioned at the same distance from the sheets. High-speed images were recorded at the focus with and without the sheet to determine what effect the modified waveform had on the probability of generating bubble clouds.

III. RESULTS

A. Single bubble behavior

Single cavitation bubbles were observed during all pulses, regardless of whether or not a bubble cloud formed. Single bubbles appeared in random positions throughout the focus. Bubbles would usually become visible within the first or second cycle of the pulse, growing and collapsing. During this time, collapses produced shockwaves radiating from the bubble which were visible by shadowgraph. After their first collapse, bubbles typically distorted with a flattened surface proximal to the transducer. Beyond the first 1–2 cycles, the bubbles usually remained at a relatively constant radius without collapsing and emitting radial shockwaves (Fig. 3). Bubbles further distorted throughout the pulse, but the overall size remained approximately the same. Bubbles within the focus grew to radii in the range of 40–90 μm, with a mean of 65 +/− 12 μm ($n = 28$). The minimum resolvable size for the camera system at this magnification was about 5 μm. This behavior of single bubbles in response to histotripsy pulses has also been observed previously in water.[30]
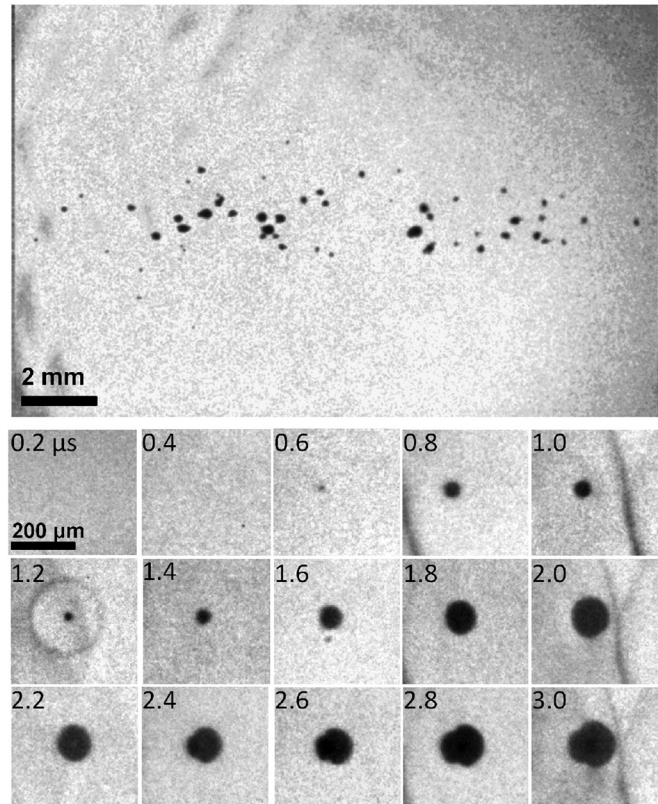

FIG. 3. Single bubbles generated at the focus of a histotripsy transducer (top) and temporal behavior of an individual bubble during the first three cycles of a pulse (bottom). Ultrasound propagation was from left to right. Bubbles appeared in the initial cycles of the pulse, and underwent inertial collapse (an emitted shockwave is visible at $t = 1.2$ μs). However, bubbles did not continue to collapse during the later cycles, but instead deformed. Note, there is some small difference in the appearance and position of the shocks (dark lines) at t = 1.0, 2.0, and 3.0 μs due to transducer ring up and camera spatial jitter.

B. Bubble cloud formation

Bubble clouds consisted of dense clusters of bubbles that formed within the focus, distinct in morphology and much larger in size than single bubbles. Not all pulses created a bubble cloud. A bubble cloud did not start to form on the first cycle, but usually began forming within 3–4 cycles. Clouds initiated from a distal position within the focal volume and grew proximally, toward the transducer (Fig. 4). Clouds grew at a nearly linear rate axially once they began to form during a pulse, but the lateral width remained constant throughout most of the pulse while the cloud was forming (Fig. 5). As shown in Fig. 5, the axial growth rate was approximately 0.5 mm/μs (i.e., $\lambda/3$ per acoustic period). This growth pattern was different from that of single bubbles, which appeared in the proximal focus before the distal focus as the pulse propagated. After the pulse passed the focus, the bubble cloud continued to expand slightly and then disappeared after 50–200 μs, depending on size of the cloud. Bubble clouds created with a greater number of cycles in a pulse were longer in dimension along the acoustic axis, but nearly identical in lateral dimension (Fig. 6). For instance, bubble clouds generated from a five cycle pulse extended 1.4 +/− 0.4 mm axially and 1.4 +/− 0.25 mm laterally, while clouds from a 20 cycle pulse were 4.8 +/− 1.1 mm axially and
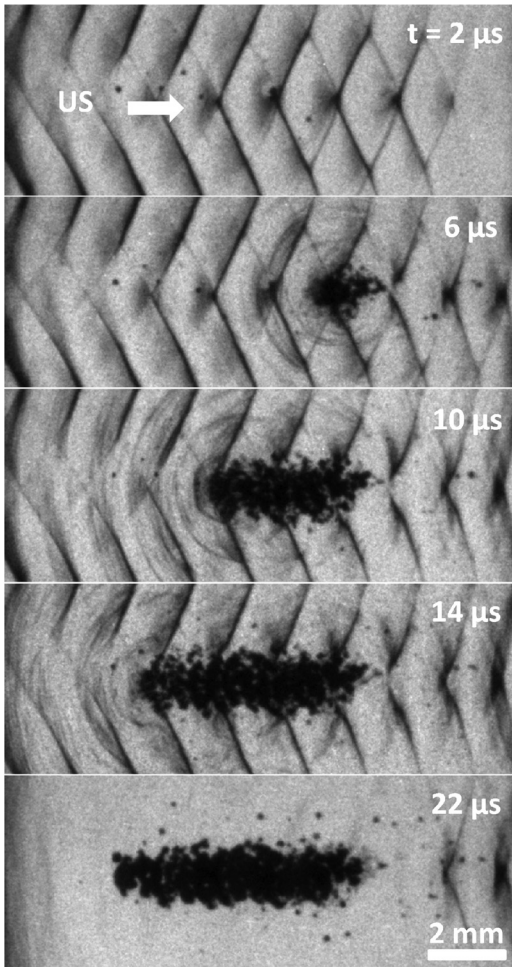
FIG. 4. Growth of a bubble cloud at the focus during application of a 20-cycle pulse. Ultrasound propagation was from left to right. The cloud started from a distal location within the focal zone and grew toward the transducer along the acoustic axis. The dark lines in each frame are a shadowgraph pattern created by the shock fronts of each cycle of the wave.
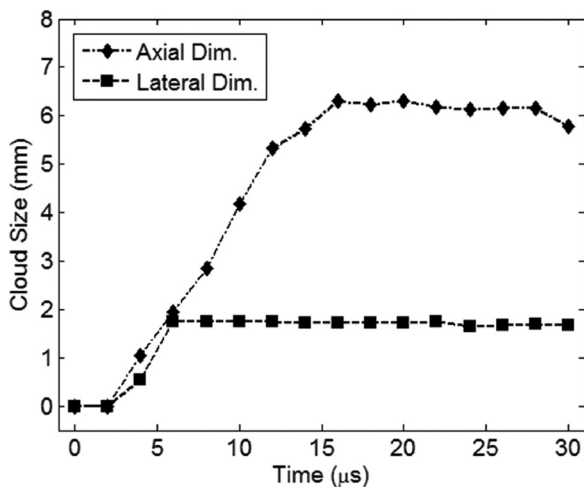

FIG. 5. Plot of measured cloud dimensions vs time for the photographic sequence in Fig. 4. The cloud started to grow between $t = 2$ and 4 μs. The time when the final acoustic cycle passed the proximal end of the cloud ($t = 16$ μs) coincided with termination of cloud growth along the acoustic axis.
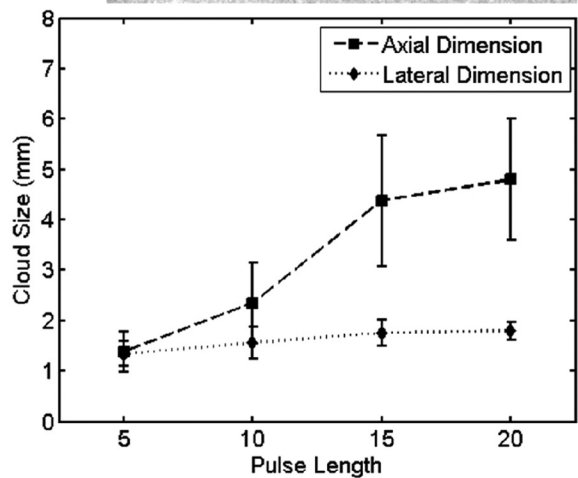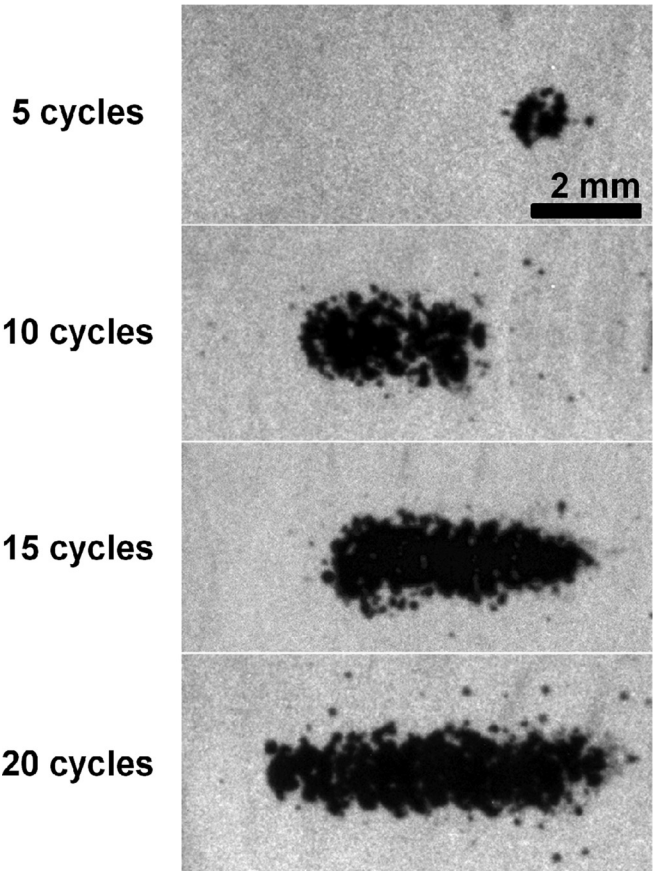

FIG. 6. (Top) Typical size and shape of bubble clouds formed during 5, 10, 15, and 20 cycle pulses at 1 MHz. Ultrasound propagation was from left to right. All images have been aligned spatially relative to the focus. Note the widths of bubble clouds were similar, but the length increased with cycle number. (Bottom) Cloud dimensions vs pulse length. The axial length of the cloud increased as the pulse length increased, but lateral size remained about the same.

1.8 mm $+/-$ 0.2 mm laterally ($n = 18$). For longer pulses (15 – 20 cycles), multiple distinct clouds would occasionally form during a single pulse, separated axially within the focal region. There were two conditions under which cloud growth would terminate. The first was when the end of the pulse completely passed the focus (i.e., sonication was terminated). The second condition occurred when the cloud extended too far proximally, outside of the focal zone.

Higher-magnification photographs of the initial formation of clouds revealed a relationship between the single

bubbles formed at the beginning of the pulse and the cavitation clouds. Cavitation clouds were always observed to stem from a single bubble after a shock front of the wave impinged on the bubble (Fig. 7). Following this event, a small cluster of cavitation appeared proximal to the bubble (cloud initiation). In Fig. 7, the initial bubble cluster propagated behind the spherically diverging wave seen at $t = 2.75$ μs. Between $t = 2.75$ and 3.0 μs, the cloud grew about 360 μm along the acoustic axis and the cloud growth velocity during this period was calculated to be 1440 m/s, which was approximately the speed of sound in the medium. The scattered wave propagated at a similar velocity. Between $t = 3.0$ and 3.25 μs, the cloud grew by 0.110 μm, and did not grow between $t = 3.25$ and 3.5 μs. In the subsequent cycle, another cluster grew after the next shock front reached the first cluster. This process continued, with clusters of cavitation forming after each cycle. Although the average cloud growth rate as shown in Fig. 5 was about 0.5 mm/μs, these results indicate that the cloud growth occurred in discrete steps with each cycle. The first cluster did not appear during the first cycle, but between cycles numbers 2–7 (mean 3.8 +/− 1.5 μs from the start of pulse, $n = 35$).
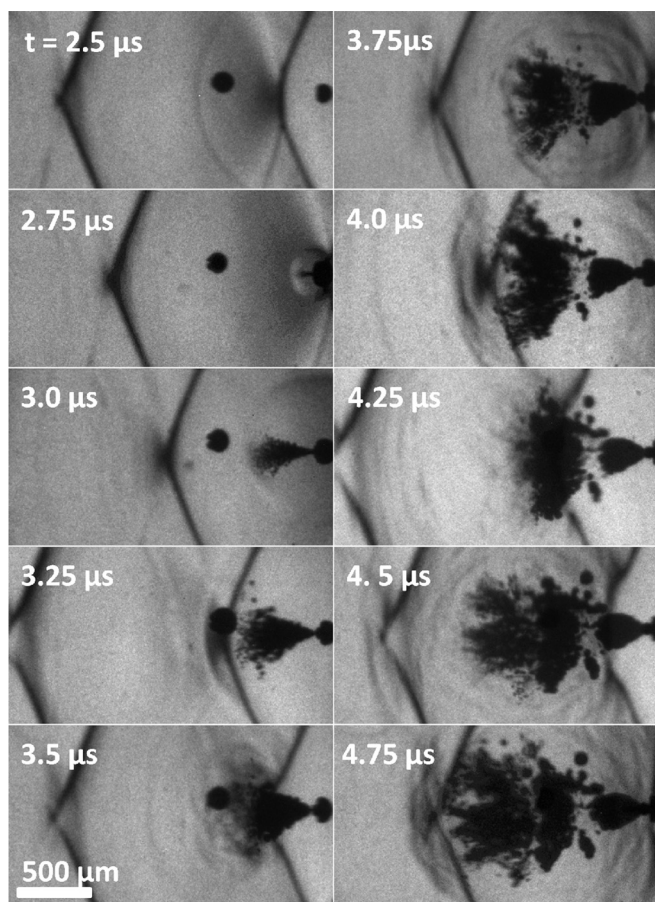

FIG. 7. Initiation of a bubble cloud. Ultrasound propagation was from left to right. At $t = 2.5$ μs, a single bubble was present at the right side of the frame. After the shock impinged on the bubble ($t = 2.75$ μs), a spherical wave was visible, apparently scattered by the bubble. Over the next cycle, a cloud of bubbles stemmed from the center of the single bubble behind this scattered wave. A second cycle produced another section of the cloud between $t = 3.5$ μs and $t = 4.0$ μs, and a third section was produced between $t = 4.25$ μs and $t = 4.75$ μs. The timing in this figure corresponded to that in Fig. 2 with the waveform at the position of the initial bubble.
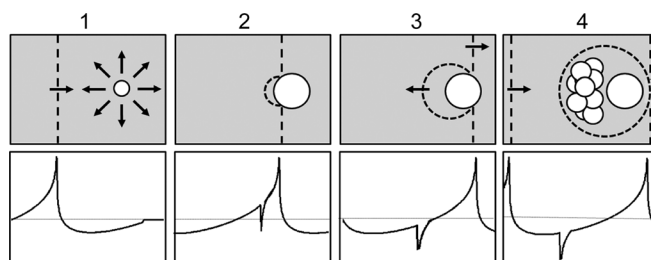
FIG. 8. Conceptual sketch of shock scattering from a bubble (top) and pressure distribution on the acoustic axis (bottom). The incident wave (shown here as a plane wave for simplicity) travels from left to right. During the initial negative phases of the pulse, single bubbles expand in response (frame 1). As a shock impinges on the bubble, the wave is scattered (frame 2). This backscattered shock constructively interferes with the incident wave to create a large transient rarefaction (frame 3). This wave induces further cavitation behind the bubble (frame 4). The next shock then scatters from this new bubble cluster, and the process repeats.

C. Mechanism of cloud formation

These observations led to the hypothesis that bubble clouds were formed by scattering of shockwaves in a pulse from the single bubbles at the focus (Fig. 8). The following is our supposition, which is tested with the results reported in the following section. The single bubbles appeared to collapse primarily during the initial cycles of the pulse. Afterward, a shock front scattered from the bubble, and no bubble collapse was observed. Because the bubble had an acoustically soft surface, the scattered portion of the pressure was inverted with respect to the incident wave, which would result in a strong tensile wave propagating back toward the transducer. We propose that this wave was responsible for forming the cavitation cluster. The following shock of the next cycle then scattered from the newly formed cluster, and created a larger cloud overall. The scattering surface grew as further cycles were applied to the proximal face of the cloud, reinforcing stronger scattering for the next cycle. This form of positive feedback was only terminated at the end of the pulse or when the proximal face of the cloud passed beyond the focus, where the pressure was too low to create significant scattering.

D. Evaluation of cloud formation mechanism

The proposed mechanism suggested that the rarefaction phase of the incident wave formed single bubbles, while the compressive shock was the source of scattering and the ensuing cavitation cloud. The experiments below were performed to determine the contribution of waveform asymmetry caused by nonlinearity and the positive phase of the wave to forming bubble clouds.

1. Cloud formation position

If cloud formation is dependent on the positive pressure, the initial cloud formation position will be limited to the positive-pressure focal region instead of the negative-pressure focal region. The locations of single bubbles that initiated cloud formation were recorded (Fig. 9). All cloud initiation events occurred at the center of the focus laterally, within a range of +/− 118 μm ($n = 35$). The lateral −3 dB peak
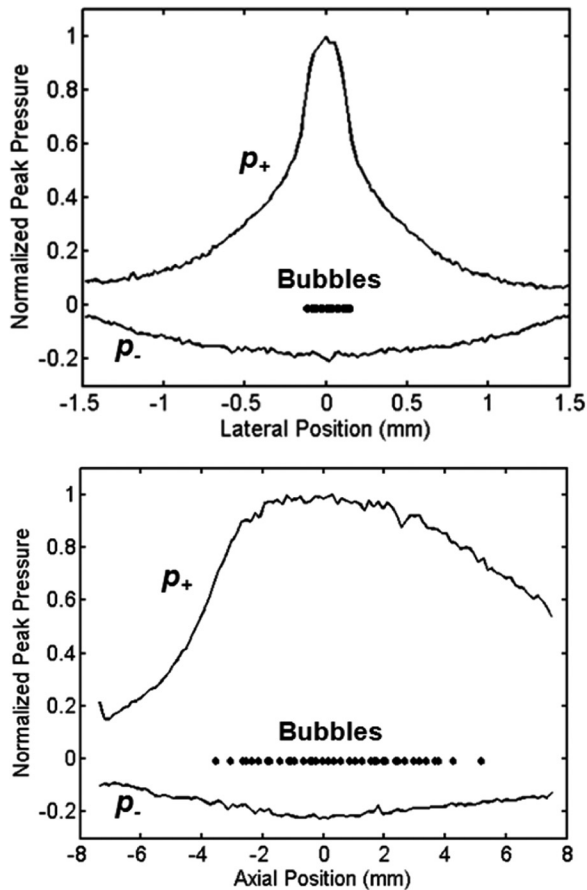
FIG. 9. Positions of bubbles (black dots, $n = 35$) for cloud initiation, as well as peak positive (p_+) and negative pressure (p_-) distribution at the focus. (Top) Lateral profile of focus and initiation bubble positions. Note bubble clouds were only formed by bubbles $+/-$ 118 μm from the center of the focus. The measured width of the -3 dB positive pressure zone at this location was 270 μm. (Bottom) Axial profile of focus and initiating bubble positions.

positive pressure width was 270 μm, and the lateral -3 dB peak negative pressure width was 1.6 mm. Axially, initiation occurred in a zone -3.5 mm prefocal to $+5.2$ mm postfocal. The axial -3 dB peak positive pressure extended from -3.5 to 5.5 mm, and from -4 to 6.3 mm for the negative pressure distribution. In this case, the -3 dB positive pressure region defined accurately the range over which initiation events were observed. The bubbles which initiated the cloud lie within the region of the focus that forms a Mach intersection,[31] due to the convergence of shock waves at the focus. This region defined the zone containing a single shock front resulting in a high peak positive pressure. Outside this region, the shock was spatially separated into two lower pressure peaks. In the outer region, the negative pressure remained nearly the same as the very center of the focus, but single bubbles visible in the outer region did not appear to create cavitation clouds.

2. Cloud formation with different waveform asymmetry

If bubble cloud formation was dependent on scattering of the positive pressure phase, then a transducer outputting a lower positive pressure level for a given negative pressure level, i.e., a lower $p_+/|p_-|$ *ratio, will have a higher threshold of negative pressure for bubble cloud formation.* Over the range of peak-negative pressure values examined in this study, the ratio $p_+/|p_-|$ was lower for the transducer with F number $= 0.6$ than for F number $= 0.9$. The probabilities of cloud formation as a function of peak negative/positive pressure are shown in Fig. 10 for both transducers in degassed water and gelatin. An S-curve was fit to each of the data sets by least-squares regression. Each curve was defined by a cumulative distribution function for a normal distribution. Table I summarizes the p_- and corresponding p_+ pressure levels at which cavitation clouds were first observed, as well as the pressure values for where the fit curve reached probability $= 0.5$. In general, cavitation clouds were observed at lower pressures with the F number $= 0.9$ transducer in both water and gelatin. However, for higher pressures ($|p_-| \geq$ 18.5) in gelatin, the probabilities for both transducers were similar (Fig. 10). Despite this, the F number $= 0.9$ transducer generated bubble clouds between $|p_-| = 13.5$–17 MPa, whereas clouds were not observed in this pressure range for the F number $= 0.6$ transducer in gelatin. These data were consistent with the hypothesis in that peak negative pressure did not solely determine the threshold for cavitation clouds, even if the frequency of the transducers and pulse length were the same.

3. Cloud formation with reduced shock amplitude

If shockwave scattering is the mechanism of cloud formation, then reduction of only the peak positive pressure of the incident wave will suppress cloud formation. To assess the importance of the positive phase of the wave, we used an acoustic filter to selectively prevent transmission of the higher harmonics of the shock to the focus. Without the filter in place, the peak positive/negative pressures were 85/19 MPa, and the rise time of the shock front was <8 ns. The measured rise time was limited by the bandwidth of the hydrophone in this case. When the filter was positioned about 1 cm from the focal center and the drive voltage to the transducer increased, the peak positive/negative pressure was 38/19 MPa, and the rise time increased to 55 ns (Fig. 11). The focus shifted slightly in the lateral direction when the filter was in position, and so the lateral two-dimensional pressure distribution of the focus was recorded in each case to find the true maximum. The spatial width of the negative pressure region was also reduced slightly with the filter in place.

Without the filter, the probability of bubble cloud initiation with a 15 cycle pulse was 0.72 ($n = 101$). When the filter was inserted to reduce the shock amplitude, the probability of bubble cloud initiation was 0.01 ($n = 96$). A one-sided Z-test for the two proportions gives a p-value < 0.001. Single cavitation bubbles were visible on every pulse within the focal region in both cases. Thus, the reduction of the positive-pressure phase suppressed cloud initiation almost entirely, while single bubble cavitation was maintained.

IV. DISCUSSION

In this article, we studied the mechanism by which bubble clouds form in a tissue phantom during histotripsy using high-speed photography. Two distinct types of cavitation activity were observed: single bubble cavitation and cavitation
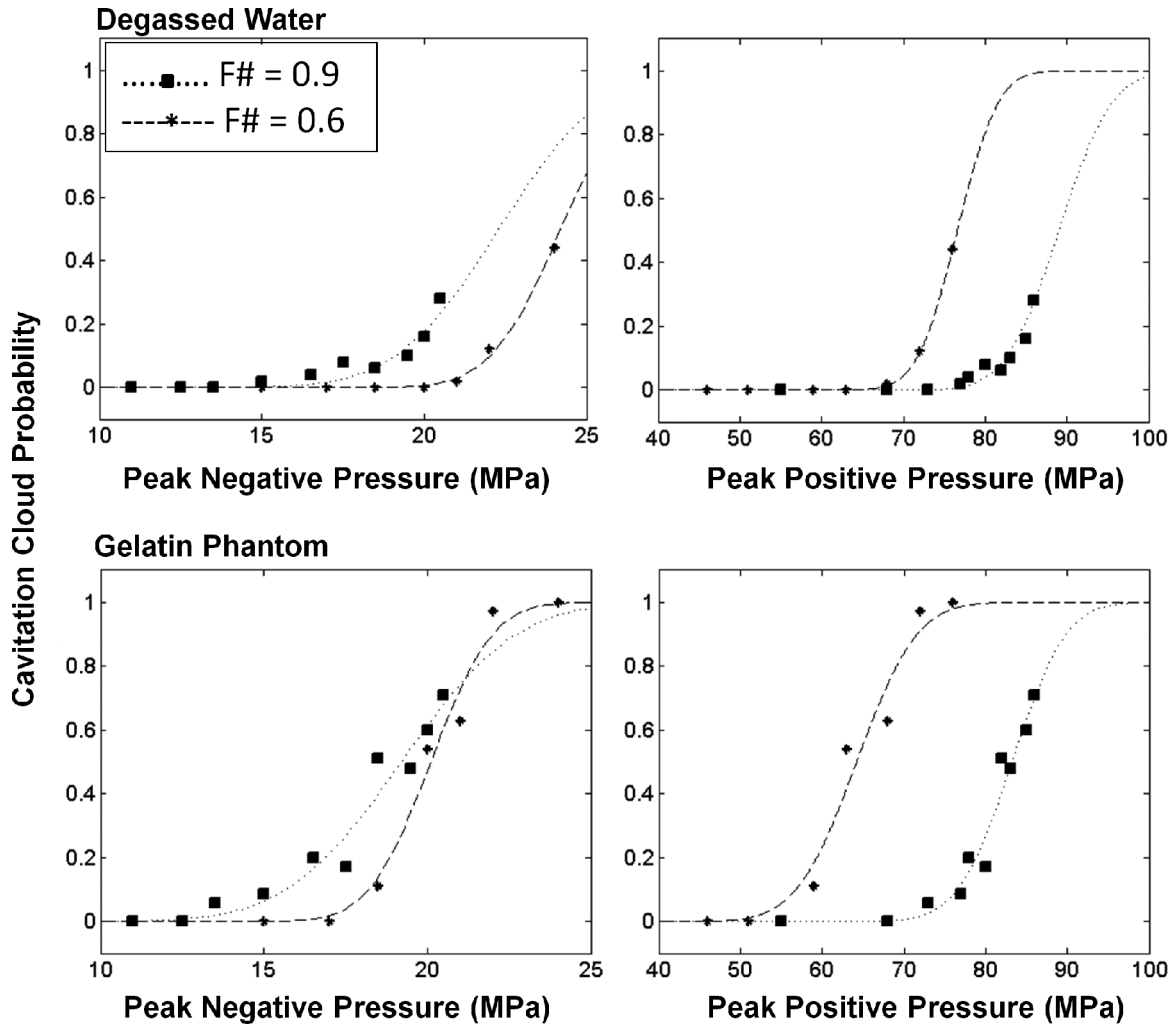
FIG. 10. Fraction of pulses that produced bubble clouds vs acoustic pressure for two different transducers with same frequency and focal length, but different F number. The upper two graphs show the bubble cloud formation probability in degassed, filtered water ($n = 50$, margin of error $= 1/\sqrt{n} = 0.14$) and the lower two graphs show the bubble cloud formation probability in gelatin ($n = 35$, margin of error $= 0.17$). Dashed lines are S-curves defined by a cumulative distribution function for a normal distribution, fit by nonlinear least squares analysis to the data.

clouds. Single bubbles were observed to grow and collapse during the initial cycles of the pulse. However, bubbles remained in an expanded state during later cycles of the pulse after they had grown to ~100 μm diameter. The lack of collapse may have resulted from the temporal asymmetry caused by nonlinearity of the waveform,[32] or the inability of the large bubble to respond within a period due to inertia. Because of this lack of collapse after the initial cycles, the cavitation bubbles acted as scatterers for the subsequent

TABLE I. Pressure thresholds for cavitation clouds with the F number $= 0.9$ and F number $= 0.6$ transducers in water and gelatin. The value p_L defines the lowest pressure at which cavitation clouds were first observed on the high-speed camera. The value p_{50} is the pressure at which the curve fits to the data in Fig. 10 give probability $= 0.5$.

		$\|p_{L-}\|$ (MPa)	$\|p_{50-}\|$ (MPa)	p_{L+} (MPa)	p_{50+} (MPa)
Water	F number $= 0.9$	15	22.3	78	89.0
	F number $= 0.6$	21	24.2	68	76.6
Gelatin	F number $= 0.9$	13.5	19.2	73	83.2
	F number $= 0.6$	18.5	20.1	60	64.2

portions of the pulse. Note that although the reflecting bubble was fairly small, its diameter being only of order of 100 μm (see Fig. 3), it was in fact large relative to the incident shock front thickness. The shock front thickness δ_s is determined by competition between the waveform steepening due to acoustic nonlinearity and smoothening due to viscosity. In classical liquids, $\delta_s = 2c(\varsigma + 4\eta/3)/(\beta \cdot p_s)$, where c is the speed of sound, ς and η are the bulk and shear viscosity coefficients, β is the parameter of acoustic nonlinearity, and p_s is the pressure jump at the shock front.[33] For instance, for water ($\varsigma = 2.5 \times 10^{-3}$ Pa s, $\eta = 1.1 \times 10^{-3}$ Pa s, $\beta = 3.5$) at $p_s = 50$ MPa, the mentioned formula gives $\delta_s \approx 0.07$ μm, which is more than 1000 times smaller than the bubble diameter, i.e., the shock reflection indeed happens as a plane wave reflection from a pressure-release mirror.

Once cavitation clouds began to form, the clouds grew along the acoustic axis at a nearly constant rate throughout the pulse. As the shockwave scattered from the proximal cloud surface, a new section of the cloud was generated with each cycle. The clouds often took on a layered structure, with small gaps without cavitation between layers separated by about 0.5 mm (near $\lambda/3$ for the fundamental frequency).
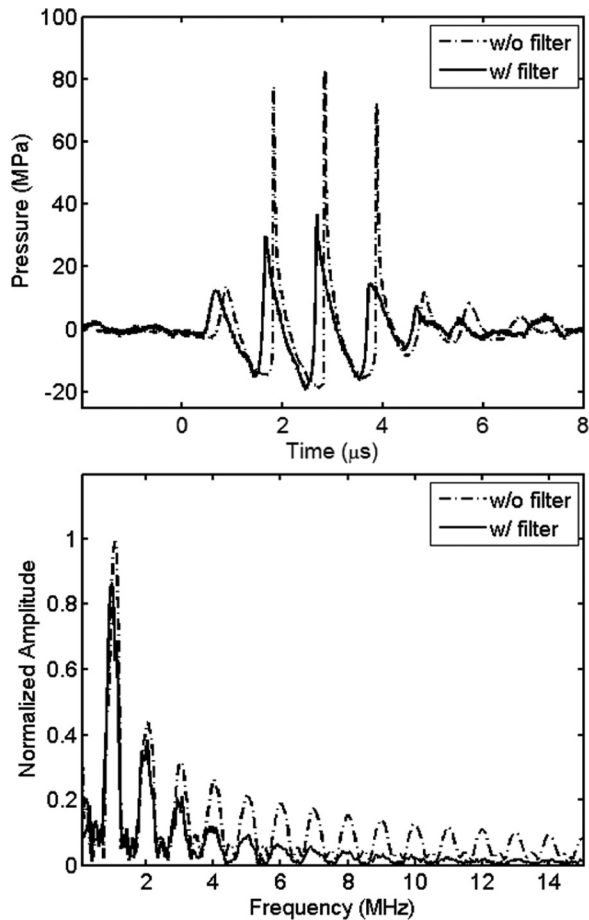
FIG. 11. Comparison of the temporal waveforms (top) and frequency spectra (bottom) with and without the acoustic filter placed between the focus and transducer. The positive pressure was lowered with the filter, while the negative pressure remained the same after increasing the transducer drive voltage. In the frequency domain, the fundamental and second harmonics had nearly the same amplitude as the original signal, but higher harmonics were greatly reduced.

This structure is evident in Fig. 7. It probably arose because of the scattering of the wave created the strongest rarefaction when it constructively interfered with the incident negative portion of the cycle, creating a position where cavitation was most dense. The process is analogous to a fracture process called spallation that plays a limited role in shock wave lithotripsy, where the wave reflects and inverts at an interface from solid to fluid or gas and fractures the distal end of the solid. However, here the wave was distorted and not sinusoidal so the constructive interference appeared near $\lambda/3$ instead of $\lambda/4$. The width and length of the cloud were limited by the focal zone, outside of which, the pressure was not sufficient to create strong scattering.

Tests to evaluate the shock scattering mechanism demonstrated the importance of the positive pressure and asymmetry caused by nonlinearity of the waveform. Clouds are initiated by bubbles within a narrow region $+/- 118$ μm from the center of the focus laterally. In this region, a single, coherent strong shock front was formed with high peak positive pressure each cycle. The focusing of shocks and the pattern observed at the focus are explained in detail by Sturtevant and Kulkarny.[33] The region of cloud initiation corresponded well with the -3 dB positive pressure region laterally

$(+/- 135$ μm), and was considerably smaller than the -3 dB negative pressure region of the focus $(+/- 800$ μm).

In another experiment, we compared the bubble cloud formation by two transducers with different F number. We observed that, in general, the lower F number transducer had higher a peak negative pressure threshold for generating bubble clouds. While the probabilities of cloud generation were similar for both transducers at $|p_-| \geq 18.5$ MPa in gelatin, clouds were only observed at $|p_-| < 18.5$ MPa with the F number $= 0.9$ transducer. It is difficult to predict the probabilities of cloud formation, since several variables, including difference in focal dimensions and different geometry of the focusing likely contribute. However, the results at lower focal pressures in gelatin, as well those in degassed water which show distinctly a lower $|p_-|$ threshold for the F number $= 0.9$ transducer lend support to the hypothesis. Meanwhile, the positive pressure level at which the clouds appeared was lower for the F number $= 0.6$ transducer than for the F number $= 0.9$ transducer. Effectively, the resulting negative pressure from the combined incident and scattered waves at their thresholds could be the same for these two different F number transducers.

In the third experiment, the positive pressure was reduced by inserting a filter plate into the focus. The higher harmonics of the wave were attenuated while the lower harmonics were transmitted to the focus. This effectively lowered the peak positive pressure at the focus and suppressed bubble cloud formation, which was consistent with the hypothesis. Since the fundamental wavelength is larger than the initial bubble and therefore does not backscatter efficiently, it is likely that scattering of harmonics generated by nonlinear propagation is most important in initiating cloud growth. However, as the cloud grows in size laterally, it may reflect lower frequencies more efficiently, and the importance of the shock may be reduced in the later cycles.

While this mechanism appears to be dominant for acoustic parameters commonly used in histotripsy, this is not the only mechanism by which bubble clouds can form. There is a similar appearance of the bubble in the third frame of Fig. 7 to that of a bubble counterjet described by Lauterborn et al.[34] It was observed that the counterjet is caused by the shock from the bubble collapse creating a small cluster of microbubbles. Despite the similarity, our experiments suggest that it was the shock from the incident wave which caused the cavitation in our case. Cavitation clouds have also been generated by applying very large tensile pulses to liquid with a single-cycle lithotripsy-type shockwave,[20] when the peak negative pressure exceeded 33 MPa. However, it is exceptionally difficult to achieve such a negative-pressure level using a harmonic waveform, because of the limits imposed by nonlinear acoustic saturation.[35,36] Alternatively, Canney et al. have demonstrated that under intense, millisecond-length focused pulses at 2 MHz, large bubbles can be achieved at the focus as a result of boiling.[37] These bubbles also demonstrate the ability to mechanically fractionate tissue. Rapid boiling is achieved primarily because of heating caused by nonlinear absorption and shockwave dissipation at the focus. Therefore, shocks also play an important role in this mechanism of bubble formation. The cavitation

clouds here also appear distinct from those observed by Willard[17] and Neppiras[18] in water under CW insonation. In liquids, it has been observed that such bubbles can proliferate into a cloud when they undergo fragmentation, either due to surface waves,[38] deformation from shockwaves, or fragmentation of the bubbles upon collapse.[39] These observations suggest that bubble clouds and mechanical tissue disruption may be achievable by several mechanisms.

Based on the understanding of this mechanism, several strategies may improve initiation of bubble clouds. The source of probability in cloud formation is ultimately related to the position and dynamic behavior of the single cavitation bubble scatterers. While it is difficult to predict where these nuclei exist *in vivo*, it may be possible to modify the therapy to improve the likelihood of cloud generation within a pulse. Injection of microbubble contrast agents could create a region more probable to generate a cloud by increasing the density of nuclei locally. If initiation is not achieved on a first pulse, then it is unlikely it will be achieved by application of further identical pulses in the same location in tissue unless a cavitation nucleus enters the focal region. It may instead be more efficient to "search" for nuclei using a spatial dithering algorithm to slightly move the focus to a new location each pulse until cloud initiation is achieved. Other strategies for efficient initiation may incorporate creation of larger scattering bubbles. A lower frequency transducer could produce larger single bubbles and provide greater degree of scattering of the wave. A higher frequency transducer could then be used to create scattering from these large bubbles and generate clouds with precision, but at a lower threshold than by itself. Such techniques may improve the reliability of bubble cloud generation, particularly in applications with small acoustic windows where it is difficult produce large focal pressures. A similar effect of large bubble creation can also be achieved through the rapid boiling mechanism when a focused transducer is excited by several millisecond duration (or longer) bursts.[37]

V. CONCLUSIONS

A mechanism of bubble cloud formation during histotripsy was proposed and investigated in this study using high-speed photography. Single bubble cavitation occurred in response to single histotripsy pulses. Bubble clouds were observed to stem from these single bubbles during the pulse, and grow along the acoustic axis, opposite the direction of ultrasound propagation. It was observed that bubble clouds began to form after a shockwave impinged on a bubble in a narrow region within the center of the focus. Based on these observations, it was proposed that the scattering of this shock creates a large transient rarefaction wave which is backscattered. The interference of this scattering with the incident wave generates a cluster of cavitation bubbles. Each subsequent cycle of the pulse then scatters and extends the cloud. This region in which clouds initiate corresponded to the area where a coherent shock front was generated at the focus. By comparing transducers of different F numbers at the same frequency, it was found that the peak rarefaction pressure of the incident wave did not indicate the threshold for cloud

cavitation. Furthermore, by reducing only the higher harmonics of the nonlinear waveform, clouds could be almost completely suppressed. These results support this mechanism, and indicate that cloud formation in histotripsy is dependent on several factors, including the location/number of existing nuclei within the tissue, both positive and negative pressure levels of the wave, and the degree of nonlinear distortion.

[1]S. Zhu, F. H. Cocks, G. M. Preminger, and P. Zhong, "The role of stress waves and cavitation in stone comminution in shock wave lithotripsy," Ultrasound Med. Biol. **28**, 661–671 (2002).

[2]Y. A. Pishchalnikov, O. A. Sapozhnikov, M. R. Bailey, J. C. Williams, R. O. Cleveland, T. Colonius, L. A. Crum, A. P. Evan, and J. A. McAteer, "Cavitation bubble cluster activity in the breakage of kidney stones by lithotripter shockwaves," J. Endourol. **17**, 435–446 (2003).

[3]S. Zhu, T. Dreyer, M. Liebler, R. Riedlinger, G. M. Preminger, and P. Zhong, "Reduction of tissue injury in shock-wave lithotripsy by using an acoustic diode," Ultrasound Med. Biol. **30**, 675–682 (2004).

[4]B. R. Matlaga, J. A. McAteer, B. A. Connors, R. K. Handa, A. P. Evan, J. C. Williams, J. E. Lingeman, and L. R. Willis, "Potential for cavitation-mediated tissue damage in shockwave lithotripsy," J. Endourol. **22**, 121–126 (2008).

[5]A. P. Evan, L. R. Willis, J. A. McAteer, M. R. Bailey, B. A. Connors, Y. Shao, J. E. Lingeman, J. C. Williams, N. S. Fineberg, and L. A. Crum, "Kidney damage and renal functional changes are minimized by waveform control that suppresses cavitation in shock wave lithotripsy," J. Urol. **168**, 1556–1562 (2002).

[6]D. L. Sokolov, M. R. Bailey, and L. A. Crum, "Dual-pulse lithotripter accelerates stone fragmentation and reduces cell lysis in vitro," Ultrasound Med. Biol. **29**, 1045–1052 (2003).

[7]R. G. Holt, and R. A. Roy, "Measurements of bubble-enhanced heating from focused, MHz-frequency ultrasound in a tissue-mimicking material," Ultrasound Med. Biol. **27**, 1399–1412 (2001).

[8]M. R. Bailey, L. N. Couret, O. A. Sapozhnikov, V. A. Khokhlova, G. ter Haar, S. Vaezy, X. Shi, R. Martin, and L. A. Crum, "Use of overpressure to assess the role of bubbles in focused ultrasound lesion shape in vitro," Ultrasound Med. Biol. **27**, 695–708 (2001).

[9]Z. Xu, A. Ludomirsky, L. Y. Eun, T. L. Hall, B. C. Tran, J. B. Fowlkes, and C. A. Cain, "Controlled ultrasound tissue erosion," IEEE Trans. Ultrason. Ferroelectr. Freq. Control **51**, 726–736 (2004).

[10]W. W. Roberts, T. L. Hall, K. Ives, J. J. S. Wolf, J. B. Fowlkes, and C. A. Cain, "Pulsed cavitational ultrasound: A noninvasive technology for controlled tissue ablation (histotripsy) in the rabbit kidney," J. Urol. **175**, 734–738 (2006).

[11]T. L. Hall, K. Kieran, K. Ives, J. B. Fowlkes, C. A. Cain, and W. W. Roberts, "Histotripsy of rabbit renal tissue in vivo: temporal histologic trends," J. Endourol. **21**, 1159–1166 (2007).

[12]Z. Xu, J. B. Fowlkes, E. D. Rothman, A. M. Levin, and C. A. Cain, "Controlled ultrasound tissue erosion: The role of dynamic interaction between insonation and microbubble activity," J. Acoust. Soc. Am. **117**, 424–435 (2005).

[13]J. B. Fowlkes and L. A. Crum., "Cavitation threshold measurements for microsecond length pulses of ultrasound," J. Acoust. Soc. Am. **83**, 2190–2201 (1988).

[14]Z. Xu, T. L. Hall, J. B. Fowlkes, and C. A. Cain, "Optical and acoustic monitoring of bubble cloud dynamics at a tissue-fluid interface in ultrasound tissue erosion," J. Acoust. Soc. Am. **121**, 2421–2430 (2007).

[15]Z. Xu, J. B. Fowlkes, and C. A. Cain, "A new strategy to enhance cavitational tissue erosion by using a high intensity initiating sequence," IEEE Trans Ultrason. Ferroelectr Freq. Control **53**, 1412–1424 (2006).

[16]H. Chen, X. Li, M. Wan, and S. Wang, "High-speed observation of cavitation bubble clouds near a tissue boundary in high-intensity focused ultrasound fields," Ultrasonics **49**, 289–292 (2009).

[17]G. W. Willard, "Ultrasonically induced cavitation in water: A step-by-step process," J. Acoust. Soc. Am. **25**, 669–686 (1953).

[18]E. A. Neppiras and W. T. Coakley, "Acoustic cavitation in a focused field in water at 1 MHz," J. Sound Vib. **45**, 341–373 (1976).

[19]M. Arora, L. Junge, and C. D. Ohl, "Cavitation cluster dynamics in shock-wave lithotripsy: Part 1. Free field," Ultrasound Med. Biol. **31**, 827–839 (2005).

[20]G. Sankin and V. Teslenko, "Two-threshold cavitation regime," Dokl. Phys. **48**, 665–668 (2003).

[21]H. Huber, K. Jochle, and J. Debus, "Influence of shock wave pressure amplitude and pulse repetition frequency on the lifespan, size and number of transient cavities in the field of an electromagnetic lithotripter," Phys. Med. Biol. **43**, 3113 (1998).

[22]G. Sankin, "Luminescence induced by spherically focused acoustic pulses in liquids," Acoust. Phys. **51**, 338–346 (2005).

[23]M. R. Bailey, D. Dalecki, S. Z. Child, C. H. Raeman, D. P. Penney, D. T. Blackstock, and E. L. Carstensen, "Bioeffects of positive and negative acoustic pressures in vivo," J. Acoust. Soc. Am. **100**, 3941–3946 (1996).

[24]C. C. Church, "A theoretical study of acoustic cavitation produced by "positive-only" and "negative-only" pressure waves in relation to in vivo studies," Ultrasound Med. Biol. **29**, 319–330 (2003).

[25]Z. Xu, M. Raghavan, T. L. Hall, M. A. Mycek, J. B. Fowlkes, and C. A. Cain, "Evolution of bubble clouds induced by pulsed cavitational ultrasound therapy - histotripsy," IEEE Trans. Ultrason. Ferroelectr. Freq. Control **55**, 1122–1132 (2008).

[26]T. Hall, and C. Cain, "A low cost compact 512 channel therapeutic ultrasound system for transcutaneous ultrasound surgery," AIP Conf. Proc. **829**, 445–449 (2006).

[27]J. E. Parsons, C. A. Cain, and J. B. Fowlkes., "Cost-effective assembly of a basic fiber-optic hydrophone for measurement of high-amplitude therapeutic ultrasound fields," J. Acoust. Soc. Am. **119**, 1432–1440 (2006).

[28]M. F. Hamilton, "Sound Beams," in *Nonlinear Acoustics*, edited by M. F. Hamilton and D. T. Blackstock (Academic, San Diego, 1998), Chap. 8, pp. 233–261.

[29]M. S. Canney, M. R. Bailey, L. A. Crum, V. A. Khokhlova, and O.A. Sapozhnikov, "Acoustic characterization of high intensity focused ultrasound fields: A combined measurement and modeling approach," J. Acoust. Soc. Am. **124**, 2406–2420 (2008).

[30]T.-Y. Wang, A. D. Maxwell, S. Park, Z. Xu, J. B. Fowlkes, and C. A. Cain, "Why are short pulses more efficient in tissue erosion using pulsed cavitational ultrasound therapy (histotripsy)?," in *9th International Symposium on Therapeutic Ultrasound,* Aix–En-Provence, France, AIP Conf. Proc. **1215**, 40–43 (2010).

[31]B. Massey and J. Ward-Smith, *Mechanics of Fluids* (Taylor & Francis, New York, 2006), Chap. 11, pp. 487–553.

[32]W. Kreider, M. R. Bailey, O. A. Sapozhnikov, V. A. Khokhlova, and L. A. Crum, "The dynamics of histotripsy bubbles," in *10th International Symposium on Therapeutic Ultrasound*, Tokyo, Japan, AIP Conf. Proc. **1359**, 427–430 (2011).

[33]B. Sturtevant and V. A. Kulkarny, "The focusing of weak shock waves," J. Fluid Mech. **73**, 651–671 (1976).

[34]W. Lauterborn and C. D. Ohl, "The peculiar dynamics of cavitation bubbles," Appl. Sci. Res. **58**, 63–76 (1997).

[35]F. A. Duck, "Acoustic saturation and output regulation," Ultrasound Med. Biol. **25**, 1009–1018 (1999).

[36]O. Bessonova, V. Khokhlova, M. Bailey, M. Canney, and L. Crum, "Focusing of high power ultrasound beams and limiting values of shock wave parameters," Acoust. Phys. **55**, 463–473 (2009).

[37]M. S. Canney, V. A. Khokhlova, O. V. Bessonova, M. R. Bailey, and L. A. Crum, "Shock-induced heating and millisecond boiling in gels and tissue due to high intensity focused ultrasound," Ultrasound Med. Biol. **36**, 250–267 (2009).

[38]T. G. Leighton *The Acoustic Bubble* (Academic, San Diego, 1994), pp. 426–427.

[39]Y. A. Pishchalnikov, J. A. McAteer, I. V. Pishchalnikova, J. C. Williams, Jr., M. R. Bailey, and O. A. Sapozhnikov, "Bubble proliferation in shock wave lithotripsy occurs during inertial collapse," in *18th International Symposium on Nonlinear Acoustics*, Stockholm, Sweden, AIP Conf. Proc. **1022**, 460–463 (2008).